Science Advances

AAAS

advances.sciencemag.org/cgi/content/full/4/3/e1701876/DC1

Supplementary Materials for

Low hydrogen contents in the cores of terrestrial planets

Vincent Clesi, Mohamed Ali Bouhifd, Nathalie Bolfan-Casanova, Geeth Manthilake, Federica Schiavi, Caroline Raepsaet, Hélène Bureau, Hicham Khodja, Denis Andrault

Published 14 March 2018, *Sci. Adv.* **4**, e1701876 (2018)
DOI: 10.1126/sciadv.1701876

This PDF file includes:

Water content determination

We employed various methods to determine the water contents of coexisting metal and silicate phases:

(i) The Al-proxy method provides the bulk water content of the sample. This method is based on the Al content of the quenched silicate phase as measured by electron probe microanalysis (EPMA), and exploits the fact that water was added to the starting material by addition of a known amount of $Al(OH)_3$. Details of this method and calibration to FTIR and Raman spectroscopic measurements are reported elsewhere (*16*).

(ii) Raman spectroscopy (see below) was performed locally on the surface of the quenched silicate phase to obtain an independent water content measurement (e.g. (*36*)). We used these measurements primarily to monitor the homogeneity of the water content in the silicate phase.

(iii) Quantitative H content measurements in both the silicate and Fe-alloy phases were obtained using elastic recoil detection analysis (ERDA, see below and Table 2). For sample W12, we could not analyze the silicate phase using ERDA, and instead use the water content determined using the Al-proxy. We report good agreement, within analytical error, between hydrogen concentrations measured by ERDA and those determined based on the Al-proxy and Raman spectroscopy (fig. S2). A similar good agreement has been reported for H contents in minerals determined by ERDA and nanoscale secondary ion mass spectrometry (nanoSIMS) (*21*).

Elastic Recoil Detection Analysis

ERDA was performed on a nuclear microprobe at LEEL CEA Saclay, equipped with a 3.5 MV Van de Graff accelerator. The incident $^4He^+$ beam of 3×3 μm^2 size was scanned over large sample areas of up to 90×90 μm^2. For extracting protons from the samples with the incident helion beam, ERDA analyses were performed with a grazing angle of 75°. Consequently, the size of the incident beam on the sample is 3×12 μm^2. The emitted H^+ ions were detected by an ERDA diode. ERDA signals (fig. S1) were processed using SIMNRA software, taking into account the sample composition (tables S2 and S3). The detection limit for H with this technique is about 54 ppm by weight H_2O (more details of H content determination by ERDA can be found elsewhere (*19,20*)). Simultaneously with ERDA, we performed particle induced X-Ray emission (PIXE), which provided Fe and Si concentration maps.

Raman spectroscopy

Raman spectroscopy was performed using a Renishaw InVia confocal spectrometer coupled with a Leica DM 2500 M optical microscope and a 532 nm diode laser. Laser

power on the sample was reduced to 15 mW and the slit aperture was set to 20 μm. We used a 100x microscope objective and a 2400 grooves/mm grating. These analytical conditions result in a spatial resolution of ~1 μm and a spectral resolution better than 1 cm^{-1}. Calibration of the spectrometer was performed based on a Si 520.5 ± 0.5 cm^{-1} peak. Raman shifts were recorded from ~100 to 1300 cm^{-1} (aluminosilicate network domain) and from ~3000 to 3800 cm^{-1} (water domain). Exposure time was set to 30 s and the number of acquisitions varied from 2 to 12, in order to improve the signal-to-noise ratio. Raman spectra were acquired at twelve different positions and depths on each sample (fig. S4a). Depth profiles between 0 (i.e., sample surface) and 2 μm depths were performed in the glass to define the depth at which the Raman signal is maximized.

Analysis of the Raman peaks was performed using the PeakFit 4.0 software. The area of the broad, asymmetric OH band centered at ~3600 cm^{-1} was calculated after subtraction of a linear baseline anchored at ~2980 and 3790 cm^{-1} (fig. S4a and S4b). In a first pass, we defined an external calibration using different standard glasses (fig. S4c), whose H_2O contents were determined in advance using FTIR and SIMS (*37*). This step provides a relationship between the peak area (i.e., the integrated intensity) of the OH band at 3600 cm^{-1} in the glass and the H_2O content (*36*). We then derived the water content of our samples based on this calibration curve (fig. S4b).

Thermodynamical model refinement for H metal-silicate partitioning

Least square refinement

Our thermodynamical model (Eq. 4) was refined by a least square regression

$$Coeff_{min} = (J^T \sigma J)^{-1} J^T \sigma K_H \quad (5)$$

In this equation, $Coeff_{min} = \begin{pmatrix} A \\ B \\ C \end{pmatrix}$ is the matrix of fitted coefficients, $J = \begin{pmatrix} \frac{1}{T_1} & \frac{P_1}{T_1} & 1 \\ \cdots & \cdots & \cdots \\ \frac{1}{T_n} & \frac{P_n}{T_{1n}} & 1 \end{pmatrix}$ the matrix of parameters (with n the number of data points), K_H the matrix of solubility coefficients, and σ the error matrix.

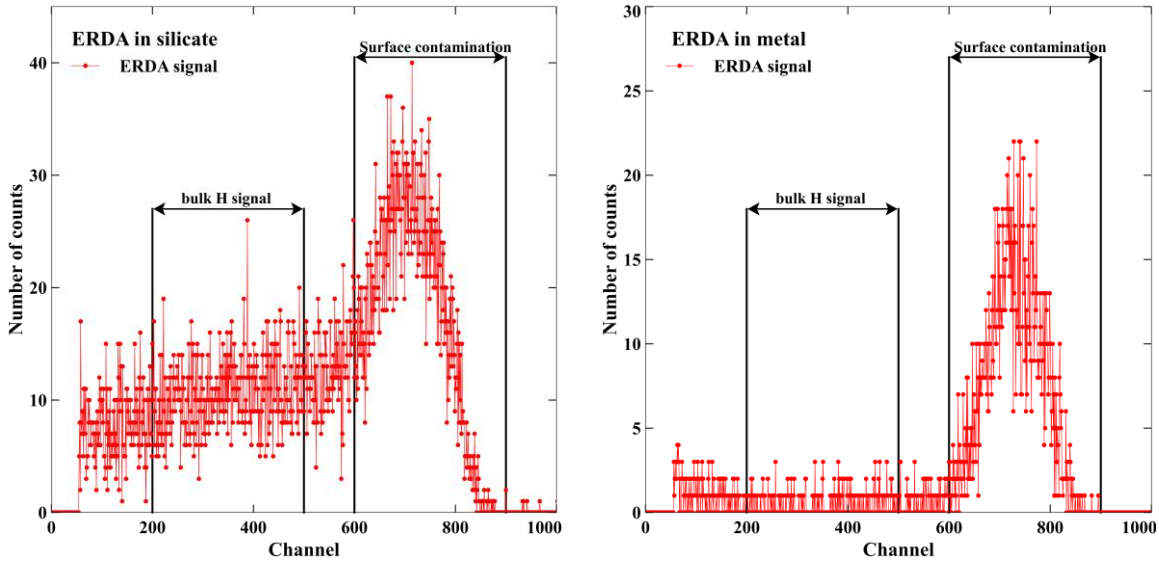

fig. S1. ERDA signal in quenched silicate melt (left) and metal (right) of sample SiW1. Red dots are the raw ERDA signal, which contains two regions of interest: the low-energy region (channels from ~600 to ~900) corresponds to water contamination on the sample surface, and the high-energy region corresponds to hydrogen in the analytical volume of the sample. Because the first 200 channels are not representative of hydrogen content, we used channels 200–500 to determine H content in our samples. The lithophile character of hydrogen is apparent at first glance, based on the number of counts recorded on the high energy channels of the detector ("bulk H signal"): for this sample, the detector received 10 to 20 counts per channel for the silicate phase, and between 0 to 4 counts per channel for the metal.

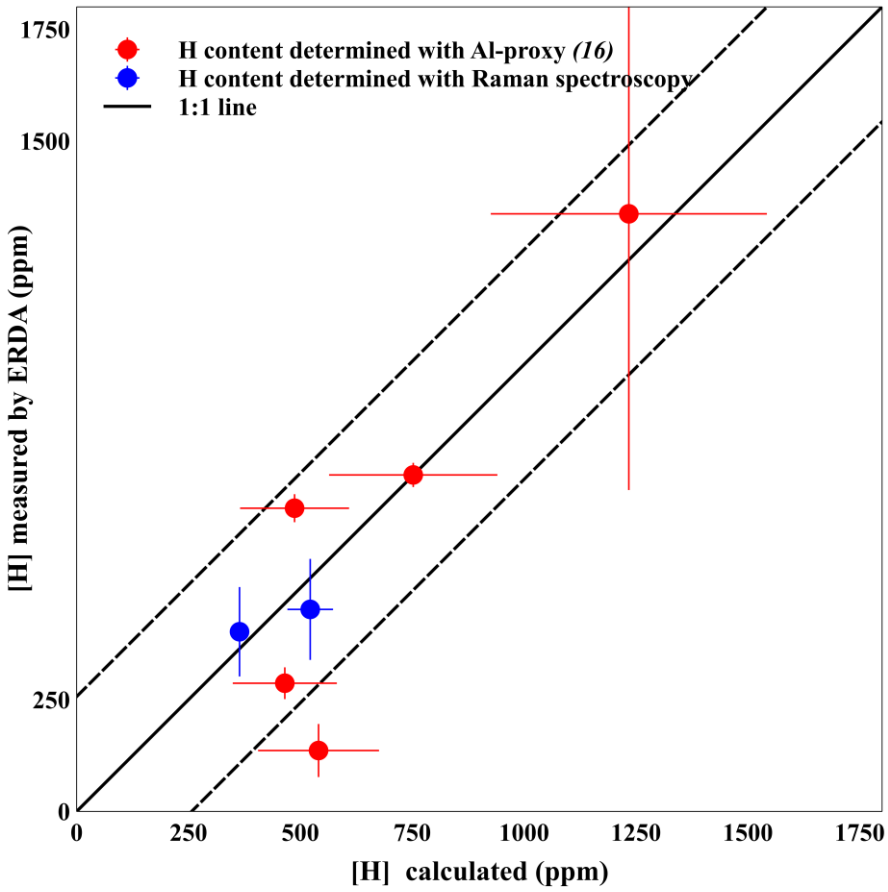

fig. S2. Comparison of H contents measured by ERDA and other techniques for determination of H content in the silicate phase. In addition to ERDA, we measured water contents using Raman spectroscopy at the same sample position (blue dots) and the Al-proxy (red dots; see Methods). Black solid and dashed lines are the 1:1 regression and 1σ uncertainty for H contents (±250 ppm), respectively. We note that amount of H found in the recovered silicate phases is similar to the bulk amount of H of the starting material (determined by the Al-proxy), within the uncertainties of the ERDA technique. Therefore, we discard any significant loss of hydrogen during our experiments.

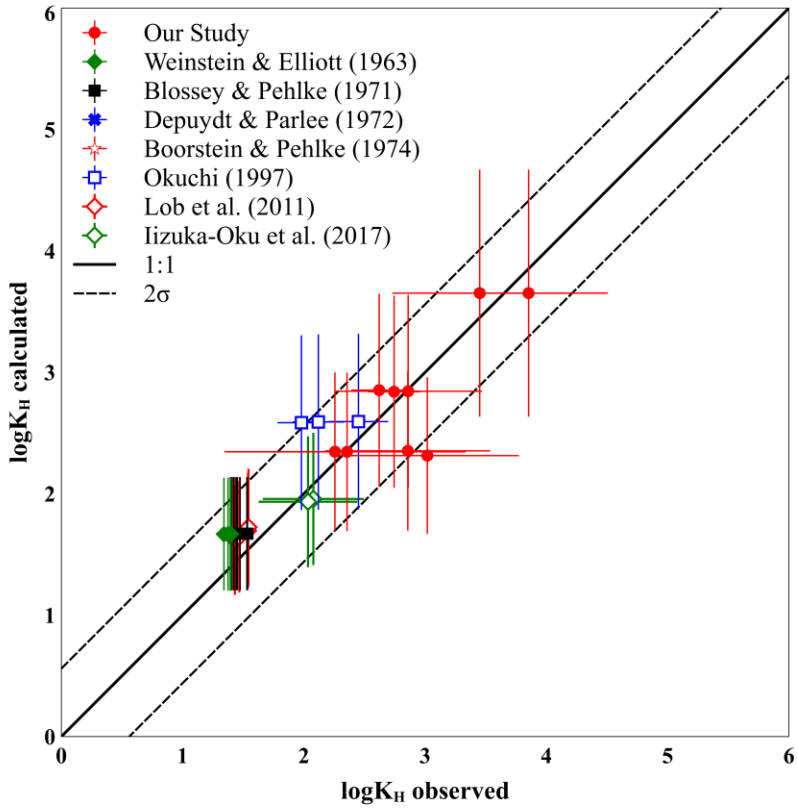

fig. S3. Comparison between experimental and theoretical K_H values. Theoretical calculations were performed using Eq. 4, with coefficients A, B, and C refined using the multi-linear refinement method (Eq. 5, see supplementary text). Black solid and dashed lines are the 1:1 regression and 2σ uncertainties, respectively. The K_H measured is calculated from the composition of metallic phase, interaction parameters and hydrogen fugacity in the silicate or the gases. The calculation of hydrogen fugacity for silicate is explained in the thermodynamical modeling. Given the few number of data point (especially at high pressure) and the high errors on the measure of hydrogen in the metal (fig. S2), the 95% confidence interval (2σ) is large, and it yields predictive results for H concentration in a metallic phase accurate within 50% of uncertainty. The data used are from Okuchi, 1997 (*8*); Iizuka-Oku et al., 2017 (*10*); Lob et al., 2011 (*15*); Depuydt & Parlee,1972 (*18*); Weinstein & Elliott, 1963 (*38*); Blossey & Pehlke, 1971 (*39*); Boorstein & Pehlke, 1974 (*40*).

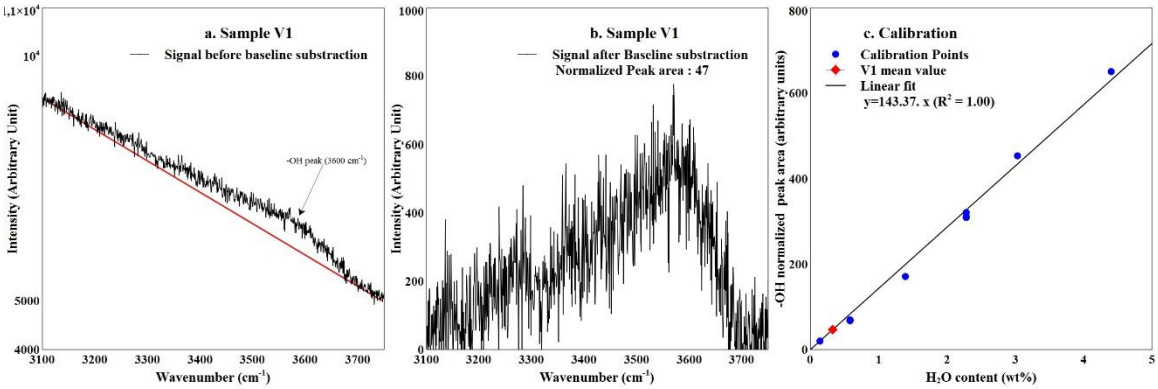

fig. S4. Example of water content determination using Raman spectroscopy. The raw signal (black) measured in the quenched silicate melt of sample V1 is shown (a) before and (b) after subtraction of the linear baseline fit between ~2980 and 3790 cm^{-1} (red line). The peak shown in (b) is the signal from structural hydrogen. The area of this OH peak is calculated using the peak-fit program. In (c), blue points are the areas of --OH Raman peaks for different standards, for which the H_2O content was previously determined (*37*). They define a calibration line (black line). The area of the --OH peak measured for sample V1 (red dot) yields a water content of 0.33 ± 0.06 wt% (corresponding to 362 ± 65 ppm H) in the silicate phase.

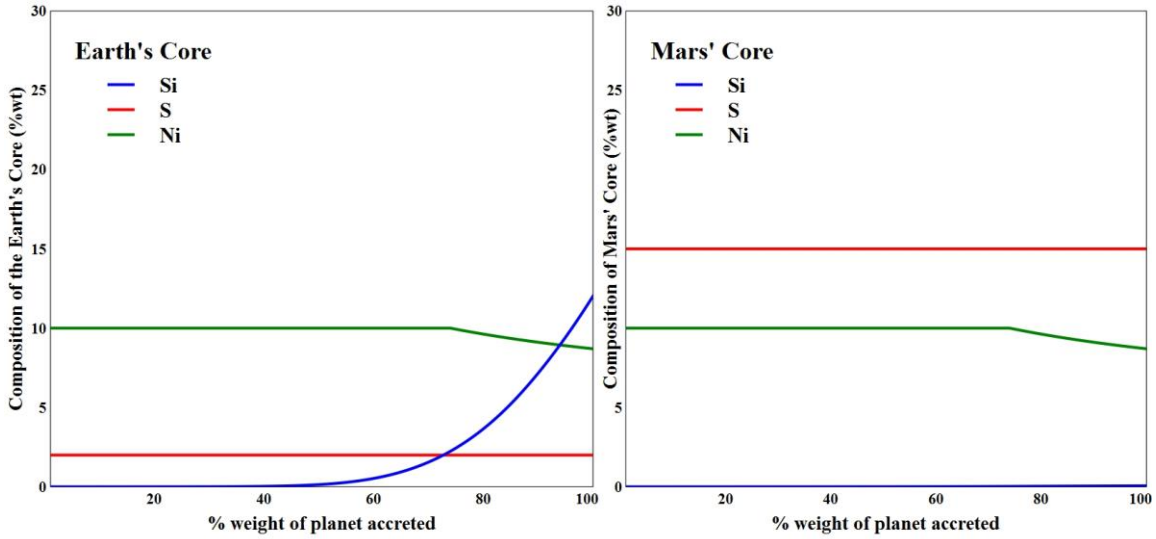

fig. S5. Evolution of the core compositions of Earth (left) and Mars (right) during the course of planetary accretion. Blue lines are silicon content, red lines are sulfur content, and green lines are nickel content. All concentrations are expressed in wt%. Si and Ni contents in both planets are calculated based on their partitioning behavior between the silicate and the metal during accretion (*16*). Due to the lack of strong geochemical constraints, we fixed sulfur contents at 2 and 15 wt% for the core of the Earth and Mars, respectively.

table S1. Composition of quenched silicate melts. Major (wt%, left portion of the table) and trace element concentrations (ppm, right portion) measured by EPMA and LA-ICPMS, respectively. Oxygen contents were derived from stoichiometry, assuming all Fe is present as Fe^{2+}. Numbers in parantheses are 1σ errors on analyses.

Element / Sample	Si	Al	Fe	Ca	Mg	V	Cr	Mn	Co	Ni	Nb	Ta	O	Total
V1	22.47	1.73	8.57	1.97	19.49	1390	1506	3987	675	451	2394	3216	43.63	99.02
	(0.15)	(0.03)	(0.07)	(0.05)	(0.29)	(16)	(37)	(43)	(25)	(56)	(10)	(28)	(0.32)	
W8	21.38	6.31	12.28	1.16	13.14	1299	1668	2273	430	183	1400	1499	42.60	97.75
	(1.06)	(0.39)	(1.34)	(0.34)	(1.77)	(88)	(151)	(43)	(62)	(35)	(12)	(22)	(1.81)	
W16	23.35	2.14	7.88	1.92	18.84	1561	1841	4083	409	198	2439	2652	43.81	99.26
	(0.26)	(0.12)	(0.31)	(0.07)	(0.15)	(22)	(47)	(11)	(20)	(69)	(232)	(89)	(0.43)	
W12	18.80	4.59	13.51	1.74	16.22	1914	2456	3488	679	436	2068	2104	40.75	96.93
	(1.54)	(0.60)	(1.42)	(0.14)	(1.41)	(589)	(915)	(922)	(159)	(88)	(242)	(220)	(2.86)	
W19	19.20	7.69	18.55	0.47	16.13	1689	2711	3504	881	630	2053	1849	41.90	99.51
	(0.43)	(0.52)	(1.13)	(0.12)	(0.13)	(73)	(778)	(159)	(89)	(27)	(221)	(191)	(1.72)	
W34	18.52	4.57	9.87	1.45	16.34	1282	5199	3178	1316	1551	1401	1298	39.41	96.50
	(0.34)	(0.21)	(0.43)	(0.20)	(0.34)	(64)	(405)	(81)	(70)	(128)	(120)	(106)	(0.69)	
SiW1	29.71	2.25	0.63	1.89	17.59	71.55	162	1720	19.4	10.4	9.5	168	48.37	100.66
	(0.14)	(0.04)	(0.08)	(0.03)	(0.16)	(2.23)	(32)	(12)	(3.6)	(2.9)	(1.3)	(1.6)	(0.71)	
SiW8	23.87	2.43	0.69	0.86	22.62	232	356	1977	116	369	50	438	44.83	95.65
	(1.20)	(0.16)	(0.06)	(0.07)	(1.22)	(126)	(142)	(920)	(42)	(81)	(25)	(195)	(19.7)	
SW3	13.38	6.11	26.33	0.22	15.75	2125	n.d.	1802	1410	353	n.d.	516	38.69	101.12
	(1.20)	(1.59)	(1.68)	(0.19)	(1.48)	(14)		(48)	(67)	(48)		(100)	(1.59)	

"n.d." stands for not detected.

table S2. Composition of metals. Major (wt%, left portion of the table) and trace element concentrations (ppm, right portion) measured by EPMA and LA-ICPMS, respectively. Numbers in brackets are 1σ errors on analyses.

Element / Sample	Fe	Ni	Co	Si	S	V	Cr	Mn	Nb	Ta	C[1]
V1	81.77 (0.26)	8.70 (0.32)	4.43 (0.10)	0.07 (0.12)	-	683 (22)	1627 (54)	102 (4)	154 (48)	12 (0.42)	4.76
W8	80.75 (1.63)	9.59 (1.67)	4.17 (0.18)	0.01 (0.01)	-	194 (63)	418 (49)	208 (75)	142 (54)	135 (50)	5.48
W16	83.01 (0.21)	8.37 (0.24)	4.21 (0.06)	0.014 (0.0007)	-	169 (14)	530 (200)	21 (0.43)	24 (21)	2 (1)	4.86
W12	80.58 (0.64)	9.37 (0.75)	4.35 (0.16)	0.018 (0.004)	-	80 (10)	444 (47)	34 (2)	7.9 (0.2)	0.44 (0.03)	5.69
WMA19	80.34 (0.23)	10.2 (0.24)	4.13 (0.06)	0.012 (0.0007)	-	648 (40)	2832 (153)	230 (28)	45.9 (6.3)	2.8 (0.2)	5.74
WMA34	81.06 (0.46)	7.90 (0.40)	3.93 (0.07)	0.03 (0.03)	-	150 (27)	2390 (0.01)	155 (19)	11.69 (0.003)	242 (25)	7.50
SiWMA1	76.72 (0.33)	8.06 (0.24)	3.56 (0.11)	8.68 (0.29)	-	1492 (41)	2018 (77)	1236 (59)	1634 (35)	1565 (28)	2.99
SiWMA8	77.62 (0.25)	8.70 (0.05)	3.26 (0.07)	5.10 (0.06)	-	3970 (85)	7217 (2920)	5051 (28)	n.d.	n.d.	5.43
SWMA3	65.21 (1.25)	3.71 (0.28)	n.d.	0.01 (0.001)	27.22 (0.77)	n.d.	n.d	n.d.	n.d.	n.d.	4.12

"n.d." stands for not detected.

[1] Carbon contents are calculated as the difference between 100% and the sum of all other element concentrations, assuming negligible O content.

table S3. Interaction parameters between hydrogen and each element *i* present in the metal [from (*15*)]. $\varepsilon^{i}_{H}(T_0)$ is reported for the reference temperature T_0 = 1592 °C. Interaction parameters (ε^{i}_{H}) for our Fe-alloys at experimental conditions were calculated using $\varepsilon^{i}_{H}(T) = (T_0/T)\cdot\varepsilon^{i}_{H}(T_0)$.

Element *i*	$\varepsilon^{i}_{H}(T_0)$
Ni	-0.00116
Co	0.00075
Si	0.026
S	0.0174
C	0.065